

Supporting Information

Strong electrostatic adsorption-engaged fabrication of sub-3.0 nm PtRu alloy nanoparticles as synergistic electrocatalysts toward hydrogen evolution

Zhipeng Yang ^a, Dandan Yang ^a, Yi Wang ^a, Yan Long ^a, Wenchao Huang ^{b, *} and Guangyin Fan ^{a, *}

^a College of Chemistry and Materials Science, Sichuan Normal University, Chengdu 610068, China

^b College of Materials Science and Engineering, Chongqing University of Technology, Chongqing 400054, China

* Corresponding author

Email: sky_hj38@163.com (W. Huang); fanguangyin@sicnu.edu.cn (G. Fan)

Materials and chemicals

Tris (2,2'-bipyridine) dichlororuthenium (II) hexahydrate, Chloroplatinic acid hexahydrate ($\text{Pt} \geq 37.5\%$) were purchased from Aladdin Industrial Corporation. Ruthenium(III) chloride trihydrate was purchased from Inno Chem Corporation. Ethanol (99%) and Ethylenediamine tetra-acetic acid tetra-sodium salt (Na_4EDTA , $\text{C}_{10}\text{H}_{12}\text{N}_2\text{Na}_4\text{O}_8 \cdot 4\text{H}_2\text{O}$) were purchased from Chengdu Ke Long Chemical Reagent Factory. Ultrapure deionized water (Milli-Q, resistivity of 18.2 M Ω , total organic carbon of 2 ppb) was used for the synthesis of catalyst and the preparation of electrolytes.

Synthesis of the Na_4EDTA -derived carbon (EC)

The synthesis of Na_4EDTA -derived carbon was achieved by the method reported previously.¹ Transfer the crucible containing 5.0 g Na_4EDTA to the muffle furnace and heated to 700°C for 4 h. Then, the products were washed with dilute hydrochloric acid and deionized water. Finally, Na_4EDTA derived carbon was dried in an oven overnight.

Synthesis of $[\text{Ru}(\text{bpy})_3][\text{PtCl}_6]$ compound (PtRu compound).

Typically, 0.05 mmol of Tris (2,2'-bipyridine) dichlororuthenium (II) hexahydrate was dissolved in 3 mL of ethanol (99.9%). Then, the solution passes through ultrasound to form a red solution. Into the red solution, 3 mL ethanolic solution of 0.05 mmol of $\text{H}_2\text{PtCl}_6 \cdot 6\text{H}_2\text{O}$ was added instantly. Orange PtRu compound was precipitated right after the addition of Pt solution. Then, the precipitate was separated by centrifugation and dried in oven overnight, respectively.

Synthesis of PtRu/EC

The 8.1 mg freshly prepared PtRu compound was dispersed in the 15 ml water. The resulting mixture was sonicated for 10 min and stirred for 2 h, after which 10 mL of aqueous EC solution (4 mg/mL) was added dropwise. The PtRu compound was well attached on EC after mixing them for 5 h followed by freeze-drying. The composite containing PtRu compound grains on EC was then thermally treated at different temperatures for 7 h in argon flow, during which a complete wetting and decomposition of PtRu compound occurs on the surface of EC, forming atomically ordered PtRu alloy nanoparticles on EC denoted as PtRu/EC. The fabricated samples were denoted as PtRu/EC-x (x is thermally treated temperature).

Synthesis of Pt/EC-700 and Ru/EC-700

Pt/EC-700 and Ru/EC-700 were prepared following the same protocol for the synthesis of PtRu-700 except that PtRu compound was used in place of $\text{H}_2\text{PtCl}_6 \cdot 6\text{H}_2\text{O}$ and $\text{RuCl}_3 \cdot 6\text{H}_2\text{O}$.

Characterization:

Scanning electron microscope (SEM, JSM-7500, Japan) was used to characterize the morphology of the obtained samples. X-ray diffraction (XRD) was executed on a Regaku D/Max-2500 diffractometer. X-ray photoelectron spectroscopic (XPS) spectra were measured on a Thermo ESCALAB 250 Axis Ultra spectrometer. Transmission electron microscopy (TEM, JEM-2100F, JEOL) was used to measure the morphology and microstructure of PtRu/EC-700. SEM-mapping and Energy dispersive X-ray

spectroscopy (EDS) was conducted on Oxford instrument operating at 200 kV. The inductively coupled plasma mass spectrometry (ICP-MS) was executed on an Agilent Technologies 8900 equipment.

Electrochemical measurements:

The electrochemical measurements were carried out on an electrochemical workstation (CHI 760E). All HER measurements were carried out on a standard three-electrode system which consists of carbon cloth as the working electrode, Hg/HgO (saturated calomel) as the reference electrode, and graphite rod as the counter electrode. The electrolyte is 1.0 M KOH. To prepare the working electrode (WE): 2.0 mg of catalyst was added into the solution containing 800.0 μL of ethanol and 10.0 μL of 5% Nafion, and the mixture was ultrasonically dispersed for a period of time to form a homogeneous suspension. Afterward, 100.0 μL of catalyst ink was loaded as evenly as possible on the carbon cloth (0.25 cm^2). All the linear sweep voltammetry (LSV) curves were represented with 90% iR-compensation. The scan rate was 5 mVs^{-1} used for linear sweep voltammetry tests. In all measurements, the potential in the 1 M KOH was calibrated to the RHE by using the following Nernst equation: $E^\ominus (\text{vs RHE}) = E^\ominus (\text{vs Hg/HgO}) + 0.8288 \text{ V}$. The long-term cyclic voltammetry tests (CV) tests was carried out in the potential range from -10 mV to -50 mV vs RHE with a scan rate of 50 mV/s . The linear portions of Tafel plots under small overpotentials were fitted to the Tafel equation: $\text{potential} = b \log(j) + a$ where a, b and j represent the standard hydrogen electrode potential, Tafel slope, and current density, respectively. The metal loadings of PtRu/EC-700 with different metal ratio were determined by ICP-MS. Surface metal

atoms on three samples were measured from XPS data (atomic percentage):

The TOF of PtRu/EC-700 can be determined from the following general equations^{2,3}:

$$\text{TOF} = j / (2 * n(\text{NM}, s) * F) \quad (1)$$

where j is the measured current density at a given overpotential (A cm^{-2}), F is the Faraday constant (96485 C mol^{-1}), the factor 2 refers to 2 electrons required to produce one H_2 molecule and $n(\text{NM}, s)$ is the number of moles of active noble metal (NM) sites per geometric surface area (mol cm^{-2}). If we assume that all NM atoms in the PtRu/EC-700 catalyst is exposed to the solution and available for the HER, then we can calculate $n(\text{NM}, s)$ from the following equation:

$$n(\text{NM}, s) = x(\text{NM}) * n(\text{catalyst}, s) = x(\text{NM}) * (\text{catalyst loading}) / M(\text{catalyst}) \quad (2)$$

$$M(\text{catalyst}) = x(\text{NM}) * M(\text{NM}) + x(\text{O}) * M(\text{O}) + x(\text{C}) * M(\text{C}) + x(\text{N}) * M(\text{N}) \quad (3)$$

In the above equation $x(\text{NM})$, $x(\text{O})$, $x(\text{N})$ and $x(\text{C})$ are the mole fractions of Pt, Ru, O, N and C, respectively, and they can be taken as the atomic percentages that are determined from the XPS analysis, while $M(\text{NM})$, $M(\text{O})$, $M(\text{N})$ and $M(\text{C})$ are the corresponding molar masses. After inserting Equations (2) and (3) in (1), we obtain the final equation for TOF calculation:

$$\text{TOF} = j / (2 * x(\text{NM}) * (\text{catalyst loading}) * F / (x(\text{NM}) * M(\text{NM}) + x(\text{O}) * M(\text{O}) + x(\text{C}) * M(\text{C}) + x(\text{N}) * M(\text{N}))). \quad (4)$$

Surface metal atoms on the sample was measured from XPS data (atomic percentage):

RuPt/EC-700: Ru: 0.42%, Pt:0.23%, C: 88.28%, O: 5.41%, N: 5.66%

$$M(\text{PtRu/EC-700}) = 0.42\% \cdot 101.07 \text{ g mol}^{-1} + 0.23\% \cdot 195.07 \text{ g mol}^{-1} + 88.28\% \cdot 12.00 \text{ g mol}^{-1} + 5.41\% \cdot 16.00 \text{ g mol}^{-1} + 5.66\% \cdot 14.00 \text{ g mol}^{-1} = 13.12 \text{ g mol}^{-1}$$

$$n(\text{NM}) = 0.65\% \cdot 9.87 \times 10^{-4} \text{ g cm}^{-2} / (13.12 \text{ g mol}^{-1}) = 4.85 \times 10^{-6} \text{ mol cm}^{-2}$$

$$\text{TOF} = 21.43 \cdot 10^{-3} \text{ A cm}^{-2} / (2 \cdot 4.85 \cdot 10^{-6} \text{ mol cm}^{-2} \cdot 96485 \text{ C mol}^{-1}) = 2.29 \text{ s}^{-1}$$

According to the XPS data. The TOF values for PtRu/EC-700, is 0.229 s⁻¹ at the overpotential of 0.03V (vs RHE).

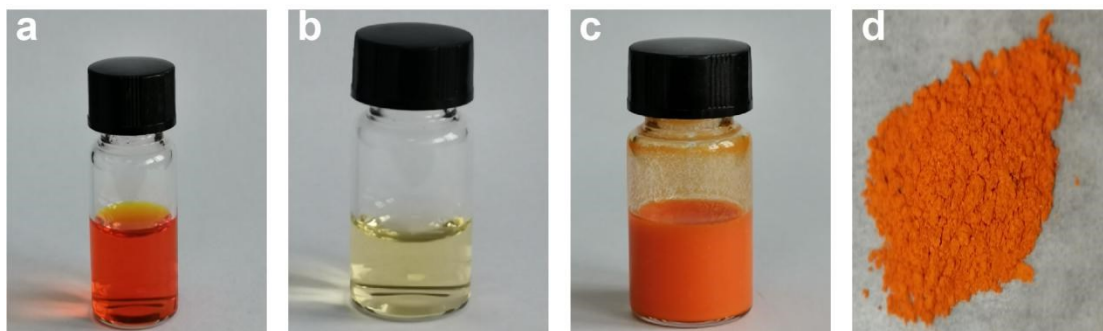


Figure S1. Photographs of (a) $[\text{Ru}(\text{bpy})_3]\text{Cl}_2$ in ethanol, (b) H_2PtCl_6 in ethanol, (c) PtRu compound in ethanol, and (d) PtRu compound after drying.

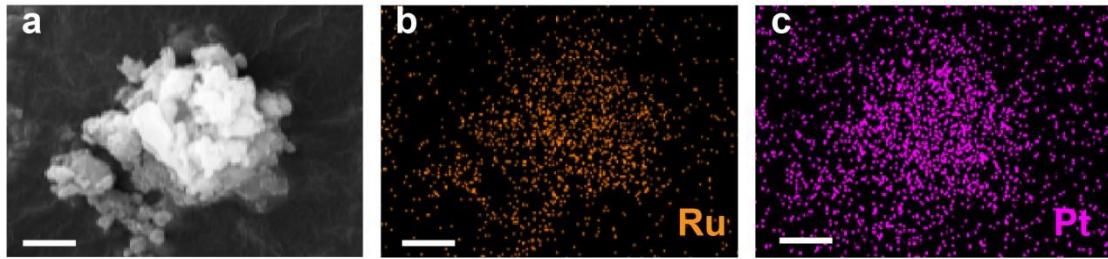


Figure S2. SEM-EDS mapping of PtRu compound.

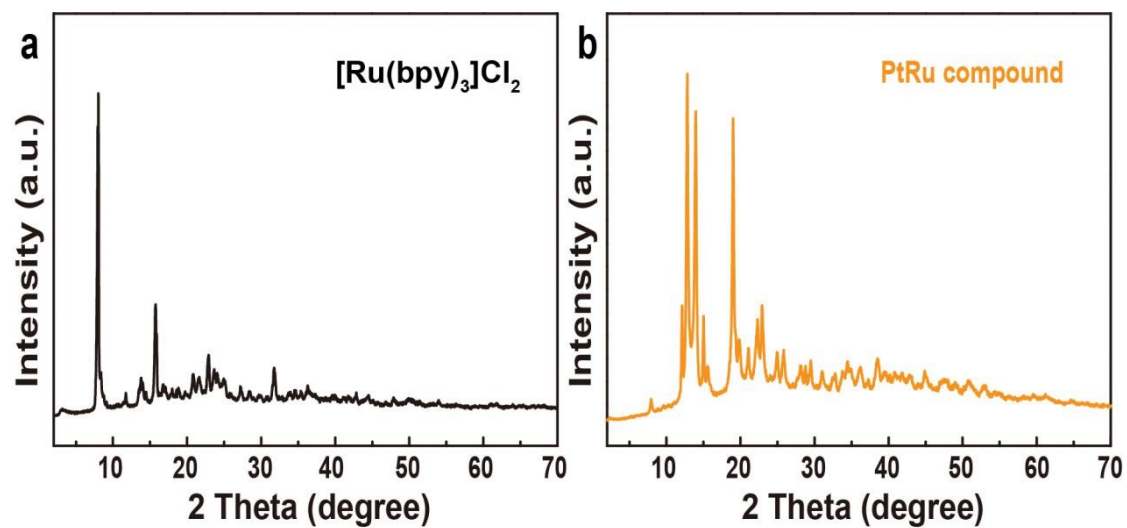


Figure S3. XRD patterns of (a) $[\text{Ru}(\text{bpy})_3]\text{Cl}_2$ and (b) PtRu compound.

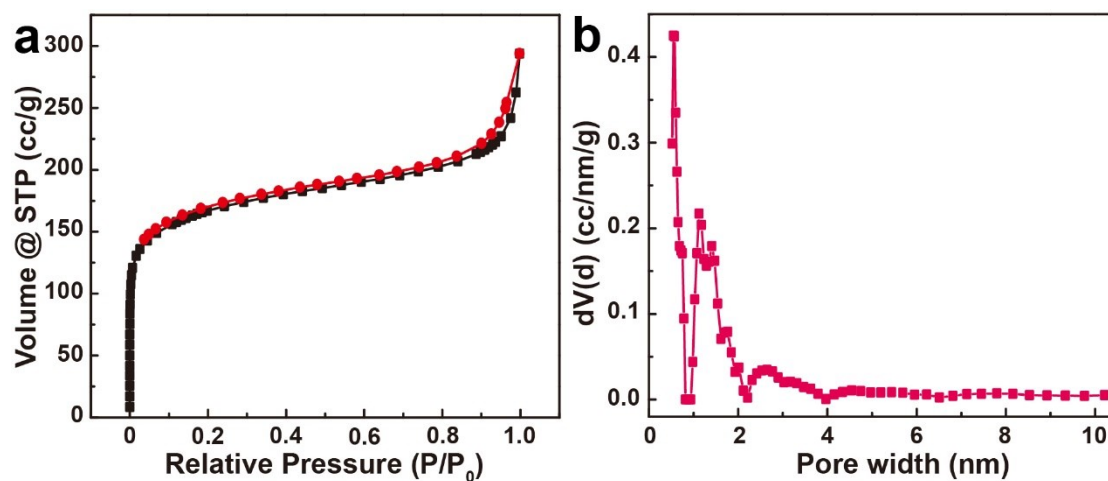


Figure S4. (a) Nitrogen adsorption–desorption isotherms and (b) pore size distribution of EC.

The isotherm profile in Figure S4a reveals that EC mainly exhibits a typical type I isotherm with a strong N_2 adsorption at low pressure, indicating that the presence of substantial micropores in the matrix. The pore size distribution in Figure S4b indicates the EC matrix are mainly composed of micropore (< 2 nm) and small mesopores (2-5 nm). The SSAs and pore volume of EC are measured to be $612.95 \text{ m}^2 \text{ g}^{-1}$ and 0.45 cc g^{-1} , respectively. Therefore, the EC matrix with abundant micro/mesopores can be utilized for the spatial confinement growth of small alloy NPs during the pyrolysis procedure.

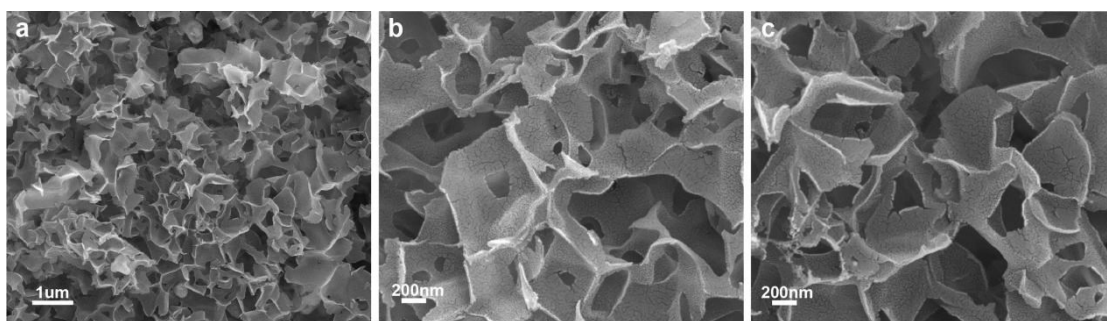


Figure S5. SEM images of (a) EC support and (b,c) PtRu/EC-700 catalyst.

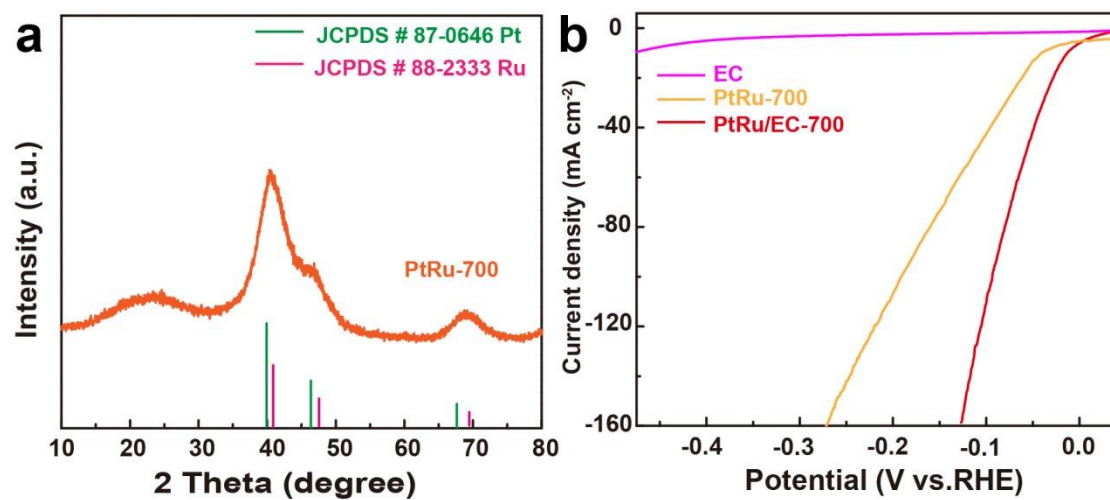


Figure S6. (a) XRD patterns of PtRu-700; (b) HER polarization curves for the as-prepared catalyst and contrast samples.

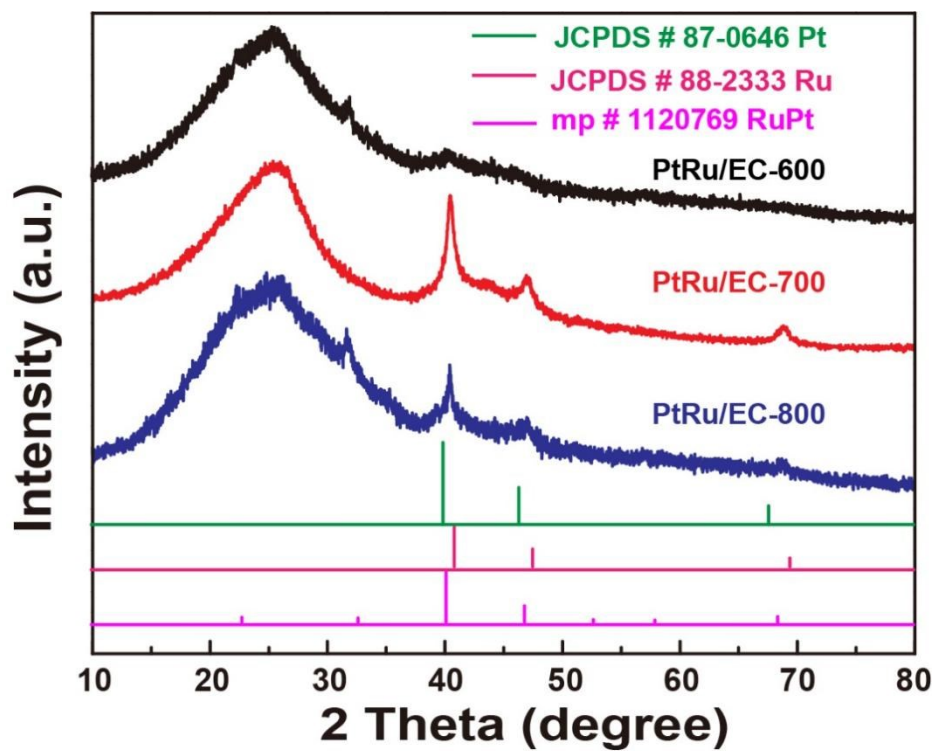


Figure S7. XRD patterns for the PtRu/EC annealed at different temperature.

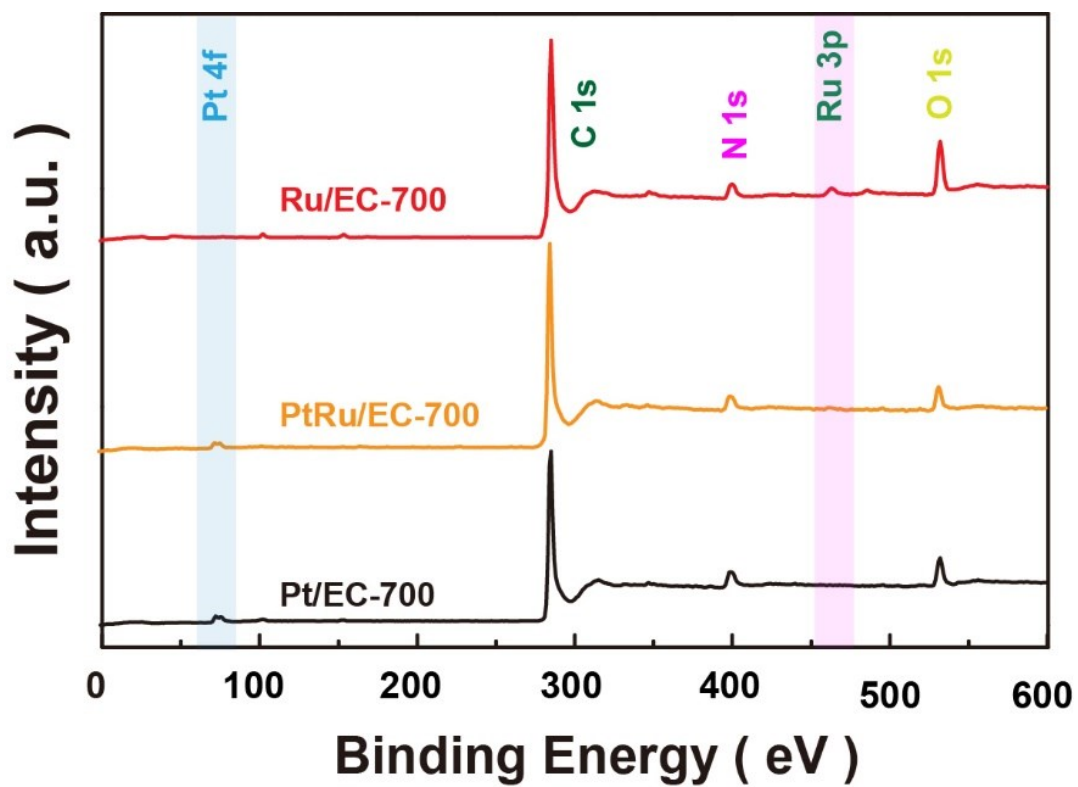


Figure S8. XPS survey spectra of the as-prepared and reference samples.

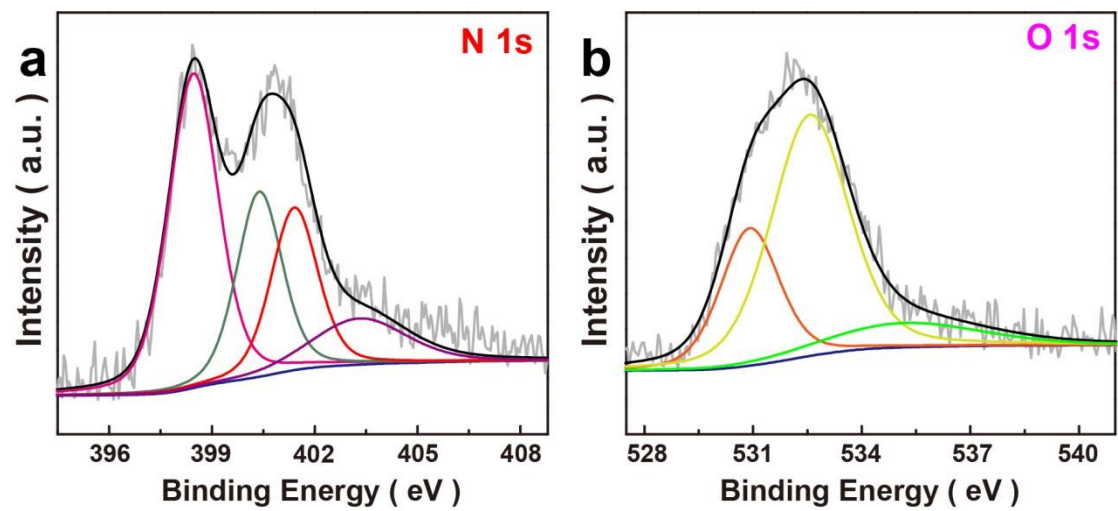


Figure S9. XPS spectra of PtRu/EC-700 (a) N 1s and (b) O 1s.

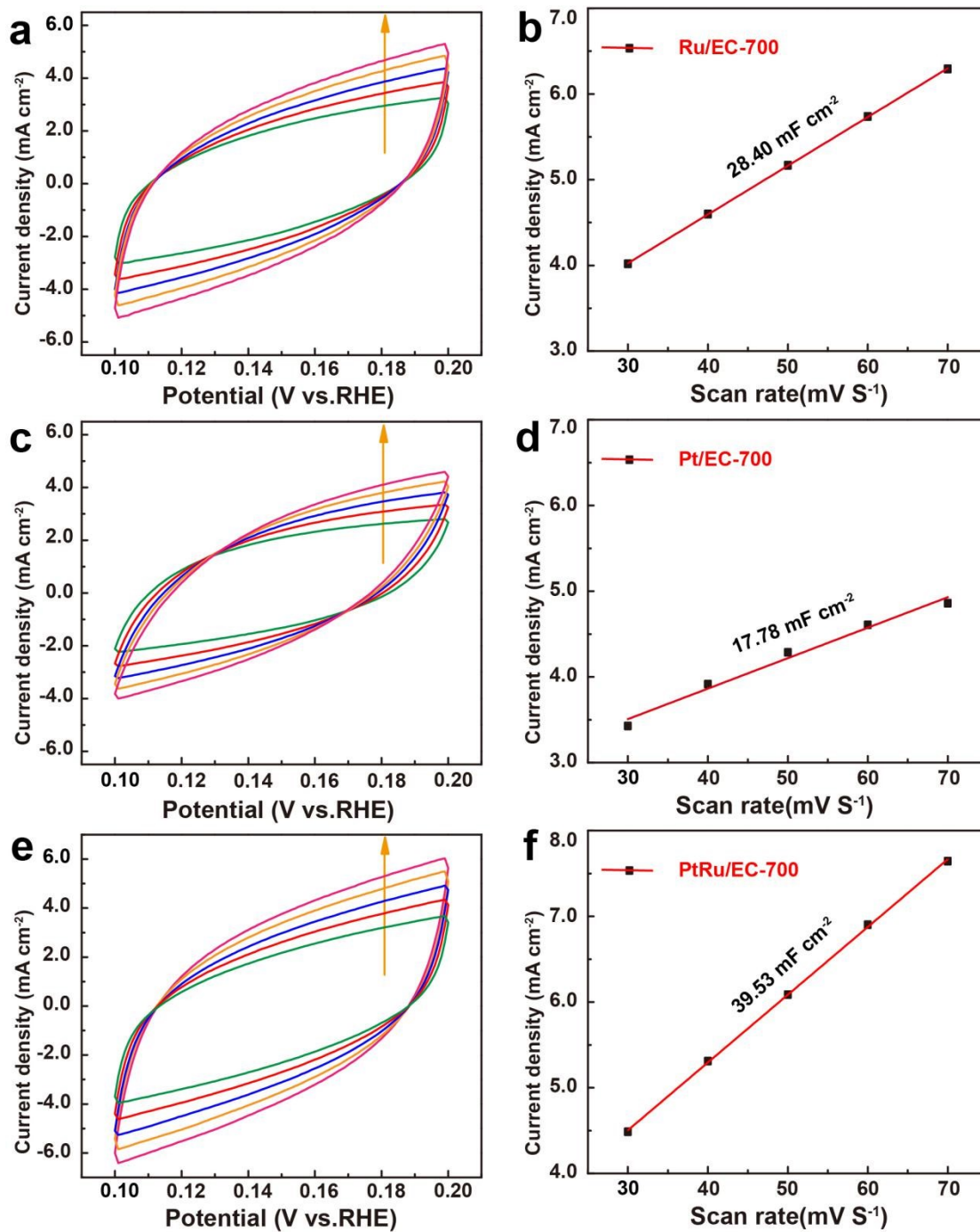


Figure S10. Cyclic voltammograms at various scan rates of 30, 40, 50, 60, 70 mV s^{-1} for (a) Ru/EC-700 (b) Pt/EC-700 and (c) PtRu/EC-700. The corresponding relationship plots between current density and scan rates for (b) Ru/EC-700 (d) Pt/EC-700 and (f) PtRu/EC-700.

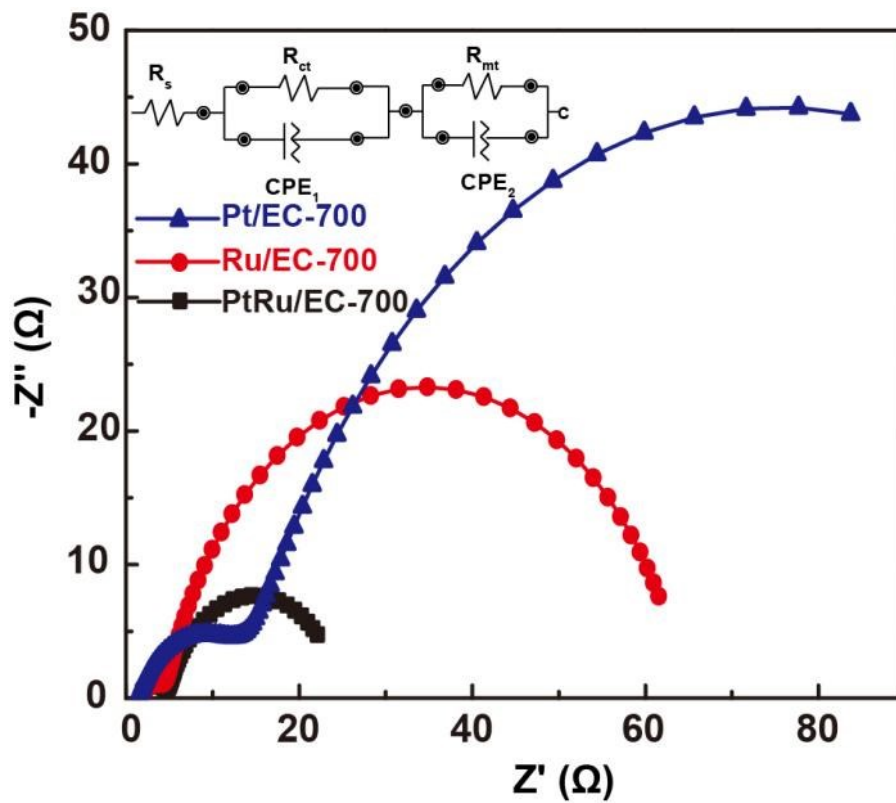


Figure S11. Nyquist plots of Ru/EC-700, PtRu/EC-700 and Pt/EC-700.

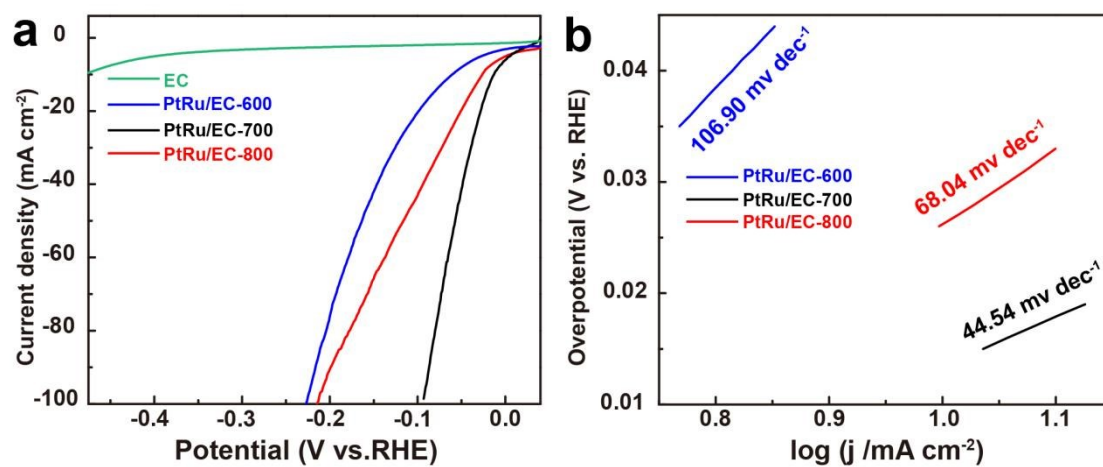


Figure S12. (a) HER polarization curves for the EC, PtRu/EC-800, PtRu/EC-700 and PtRu/EC-600 (b) Tafel plots of PtRu/EC-800, PtRu/EC-700 and PtRu/EC-600.

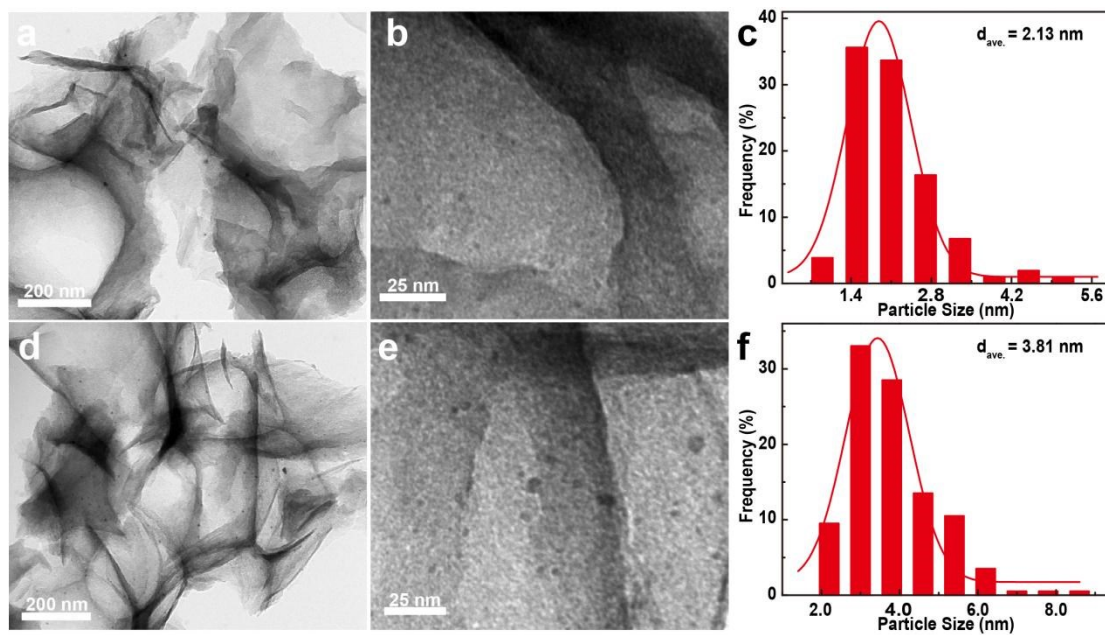


Figure S13. TEM images of PtRu/EC-600 (a,b) and PtRu/EC-800 (d,e), respectively. the size distributions of PtRu/EC-600 (c) and PtRu/EC-800 (f), respectively.

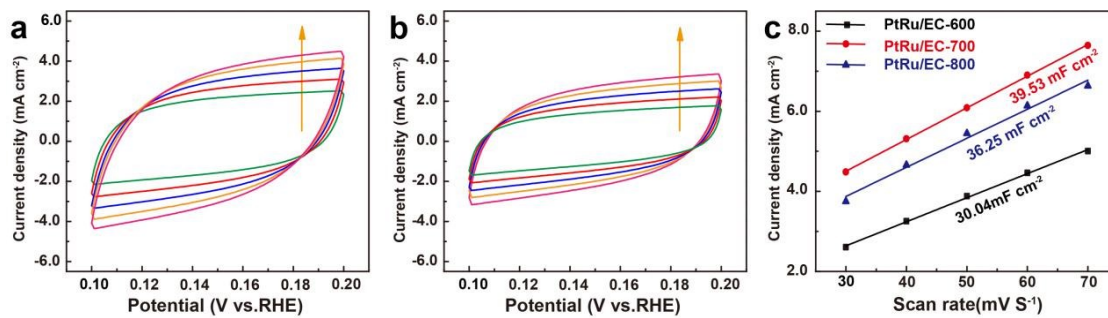


Figure S14. Cyclic voltammograms at various scan rates of 30, 40, 50, 60, 70 mV s⁻¹ for (a) PtRu/EC-800 (b) PtRu/EC-600 and (c) Capacitive current at the middle potential of CV curves as a function of scan rate.

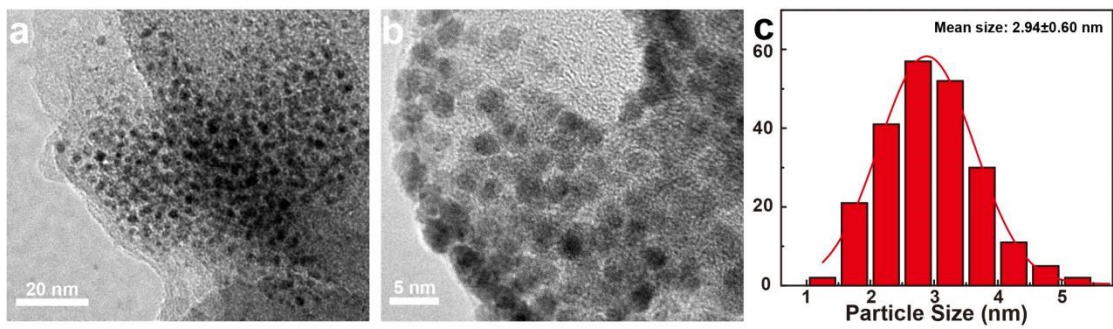


Figure S15. TEM images of PtRu/EC-700 after V-t test.

Table S1. Summary of some recently reported representative HER electrocatalysts in alkaline electrolytes.

Catalyst	Tafel slope (mV dec ⁻¹)	η_{10} (mV)	Reference
PtRu/EC-700	44.54	18	This work
RuAu-0.2	37	24	4
Ru ₂ Ni ₂ SNs/C	23.4	40	5
Ru ND/C	49	43.4	6
Ru@CN	53	32	7
Ru _{0.33} Se@TNA	50	57	8
Pd@Ru NRs	30	30	9
NiOx/Pt ₃ N	/	39	10
Ru ₂ -GC	65	25	11
RuP ₂ @NPC	52	69	12
Thick hollow Cu ₂ - xS@Ru NPs	82	48	13
2DPC-RuMo	25	18	14
RuIr@NrC	35	26	15
Pt QDs @Fe-MOF	/	33	16
h-RuSe ₂	95	34	17
PtRu NCs/BP	19	22	18
PtNi ₅ -0.3	19.2	26.8	19

Ru@WNO-C	39.7	24	20
Ru/OMSNNC	40.41	13	21
RuNi/CQDs	40	13	22
PtRu/CC ₁₅₀₀	28	19	23
Ni-doped RuO ₂ NWs	/	52	24
Ru-RuO ₂ /CNT 1	30	12	25
Sr ₂ RuO ₄	51	61	26
NiFeRu-LDH	31	29	27
NiRu@N-C	/	32	28
NiCoMo/Ru-GN	38	11.4	29
Ru ₁ Ni ₁ -NCNFs	30	35	30
RuO ₂ /N-C	44	40	31
Cu-doped	35	28	32
Ru-RuO ₂ /C			
s-RuS ₂ /S-rGO	29	25	33
Ru/np-MoS ₂	31	30	34
RhOOH NSs/C-OH-40	19.3	18	35
Pt-Ni NTAs	38	23	36
Pt-Ni heterostructure	/	48	37

References

1. W. Cheng, X. Zhao, W. Luo, Y. Wang and G. Fan, *Int. J. Hydrogen Energy* 2020, **45**, 29034-29045.
2. Y. Liu, X. Lu, Z. Che, C. Zhang, M. Han, J. Bao and Z. Dai, *Chem. Commun.* , 2018, **54**, 12202-12205.
3. P. Li, X. Duan, S. Wang, L. Zheng, Y. Li, H. Duan, Y. Kuang and X. Sun, *Small*, 2019, **15**, 1904043.
4. C.-H. Chen, D. Wu, Z. Li, R. Zhang, C.-G. Kuai, X.-R. Zhao, C.-K. Dong, S.-Z. Qiao, H. Liu and X.-W. Du, *Adv. Energy Mater.*, 2019, **9**, 1803913.
5. J. Ding, Q. Shao, Y. Feng and X. Huang, *Nano Energy*, 2018, **47**, 1-7.
6. K. Gao, Y. Wang, Z. Wang, Z. Zhu, J. Wang, Z. Luo, C. Zhang, X. Huang, H. Zhang and W. Huang, *Chem. Commun.* , 2018, **54**, 4613-4616.
7. J. Wang, Z. Wei, S. Mao, H. Li and Y. Wang, *Energy Environ. Sci.* , 2018, **11**, 800-806.
8. K. Wang, Q. Chen, Y. Hu, W. Wei, S. Wang, Q. Shen and P. Qu, *Small*, 2018, **14**, 1802132.
9. Y. Luo, X. Luo, G. Wu, Z. Li, G. Wang, B. Jiang, Y. Hu, T. Chao, H. Ju, J. Zhu, Z. Zhuang, Y. Wu, X. Hong and Y. Li, *ACS Appl. Mater. Interfaces* 2018, **10**, 34147-34152.
10. P. Wang, K. Jiang, G. Wang, J. Yao and X. Huang, *Angew. Chem. Int. Ed.* , 2016, **55**, 12859-12863.
11. J. Creus, S. Drouet, S. Suriñach, P. Lecante, V. Collière, R. Poteau, K. Philippot,

- J. García-Antón and X. Sala, *ACS Catal.* , 2018, **8**, 11094-11102.
12. Z. Pu, I. S. Amiinu, Z. Kou, W. Li and S. Mu, *Angew. Chem. Int. Ed.* , 2017, **56**, 11559-11564.
13. D. Yoon, J. Lee, B. Seo, B. Kim, H. Baik, S. H. Joo and K. Lee, *Small*, 2017, **13**, 1700052.
14. K. Tu, D. Tranca, F. Rodríguez-Hernández, K. Jiang, S. Huang, Q. Zheng, M.-X. Chen, C. Lu, Y. Su, Z. Chen, H. Mao, C. Yang, J. Jiang, H.-W. Liang and X. Zhuang, *Adv. Mater.* , 2020, **32**, 2005433.
15. J. Yu, Y. Dai, X. Wu, Z. Zhang, Q. He, C. Cheng, Z. Wu, Z. Shao and M. Ni, *Chem. Eng. J.* , 2020, DOI: <https://doi.org/10.1016/j.cej.2020.128105>, 128105.
16. B. Ye, R. Jiang, Z. Yu, Y. Hou, J. Huang, B. Zhang, Y. Huang, Y. Zhang and R. Zhang, *J. Catal.* , 2019, **380**, 307-317.
17. Y. Zhao, H. Cong, P. Li, D. Wu, S. Chen and W. Luo, *Angew. Chem. Int. Ed.* , 2021, **60**, 7013-7017.
18. Y. Li, W. Pei, J. He, K. Liu, W. Qi, X. Gao, S. Zhou, H. Xie, K. Yin, Y. Gao, J. He, J. Zhao, J. Hu, T.-S. Chan, Z. Li, G. Zhang and M. Liu, *ACS Catal.* , 2019, **9**, 10870-10875.
19. C. Zhang, X. Liang, R. Xu, C. Dai, B. Wu, G. Yu, B. Chen, X. Wang and N. Liu, *Adv. Funct. Mater.* , 2021, **31**, 2008298.
20. G. Meng, H. Tian, L. Peng, Z. Ma, Y. Chen, C. Chen, Z. Chang, X. Cui and J. Shi, *Nano Energy*, 2021, **80**, 105531.
21. Y.-L. Wu, X. Li, Y.-S. Wei, Z. Fu, W. Wei, X.-T. Wu, Q.-L. Zhu and Q. Xu, *Adv.*

- Mater.* , 2021, **33**, 2006965.
22. Y. Liu, X. Li, Q. Zhang, W. Li, Y. Xie, H. Liu, L. Shang, Z. Liu, Z. Chen, L. Gu, Z. Tang, T. Zhang and S. Lu, *Angew. Chem. Int. Ed.* , 2020, **59**, 1718-1726.
23. L. Li, G. Zhang, B. Wang, T. Yang and S. Yang, *J. Mater. Chem. A*, 2020, **8**, 2090-2098.
24. J. Wang, Y. Ji, R. Yin, Y. Li, Q. Shao and X. Huang, *J. Mater. Chem. A*, 2019, **7**, 6411-6416.
25. M. Zhang, J. Chen, H. Li, P. Cai, Y. Li and Z. Wen, *Nano Energy*, 2019, **61**, 576-583.
26. Y. Zhu, H. A. Tahini, Z. Hu, J. Dai, Y. Chen, H. Sun, W. Zhou, M. Liu, S. C. Smith, H. Wang and Z. Shao, *Nat. Commun.*, 2019, **10**, 149.
27. G. Chen, T. Wang, J. Zhang, P. Liu, H. Sun, X. Zhuang, M. Chen and X. Feng, *Adv. Mater.* , 2018, **30**, 1706279.
28. Y. Xu, S. Yin, C. Li, K. Deng, H. Xue, X. Li, H. Wang and L. Wang, *J. Mater. Chem. A*, 2018, **6**, 1376-1381.
29. R. K. Shervedani, M. Torabi and M. S. Foroushani, *J. Phys. Chem. C*, 2018, **122**, 17621-17631.
30. M. Li, H. Wang, W. Zhu, W. Li, C. Wang and X. Lu, *Adv. Sci.*, 2020, **7**, 1901833.
31. C.-Z. Yuan, Y.-F. Jiang, Z.-W. Zhao, S.-J. Zhao, X. Zhou, T.-Y. Cheang and A.-W. Xu, *ACS Sustainable Chem. Eng.*, 2018, **6**, 11529-11535.
32. K. Yang, P. Xu, Z. Lin, Y. Yang, P. Jiang, C. Wang, S. Liu, S. Gong, L. Hu and Q. Chen, *Small*, 2018, **14**, 1803009.

33. J. Yu, Y. Guo, S. Miao, M. Ni, W. Zhou and Z. Shao, *ACS Appl. Mater. Interfaces* 2018, **10**, 34098-34107.
34. K. Jiang, M. Luo, Z. Liu, M. Peng, D. Chen, Y.-R. Lu, T.-S. Chan, F. M. F. de Groot and Y. Tan, *Nat. Commun.*, 2021, **12**, 1687.
35. S. Bai, M. Xie, T. Cheng, K. Cao, Y. Xu and X. Huang, *Nano Energy*, 2020, **78**, 105224.
36. A. Nairan, C. Liang, S.-W. Chiang, Y. Wu, P. Zou, U. Khan, W. Liu, F. Kang, S. Guo, J. Wu and C. Yang, *Energy Environ. Sci.* , 2021, **14**, 1594-1601.
37. C. Zhang, B. Chen, D. Mei and X. Liang, *J. Mater. Chem. A*, 2019, **7**, 5475-5481.